



#### **OPEN ACCESS**

EDITED BY
Jie Yang,
Boston University, United States

REVIEWED BY

Yuri L. Lyubchenko, University of Nebraska Medical Center, United States Suresh Thallapuranam, University of Arkansas, United States

\*CORRESPONDENCE Luciano Saso, ☑ luciano.saso@uniroma1.it

RECEIVED 13 September 2025 ACCEPTED 16 October 2025 PUBLISHED 23 October 2025

#### CITATION

Bagheri S and Saso L (2025) Biophysical insights into the molecular mechanisms of beta amyloid aggregation and its toxic effects in Alzheimer's disease. *Front. Mol. Biosci.* 12:1704653. doi: 10.3389/fmolb.2025.1704653

#### COPYRIGHT

© 2025 Bagheri and Saso. This is an open-access article distributed under the terms of the Creative Commons Attribution License (CC BY). The use, distribution or reproduction in other forums is permitted, provided the original author(s) and the copyright owner(s) are credited and that the original publication in this journal is cited, in accordance with accepted academic practice. No use, distribution or reproduction is permitted which does not comply with these terms.

# Biophysical insights into the molecular mechanisms of beta amyloid aggregation and its toxic effects in Alzheimer's disease

Soghra Bagheri<sup>1</sup> and Luciano Saso<sup>2</sup>\*

<sup>1</sup>Medical Biology Research Center, Health Technology Institute, Kermanshah University of Medical Sciences, Kermanshah, Iran, <sup>2</sup>Department of Physiology and Pharmacology "Vittorio Erspamer", Sapienza University, Rome, Italy

Alzheimer's disease is recognized as the most common neurodegenerative disorder, characterized by the presence of amyloid plaques, which have consistently garnered significant attention. Since the disease was first identified, extensive research has been devoted to investigating these plaques. As our understanding of the disease has progressed, the detrimental role of plaques has been questioned, leading to the hypothesis that amyloid oligomeric aggregates are the main culprits. Nevertheless, subsequent research indicated that the concentrations of amyloids employed in the experiments were considerably elevated compared to physiological conditions, and that at physiological concentrations, amyloids do not exhibit significant accumulation or toxicity. This article aims to offer a detailed biophysical perspective on the formation of amyloid aggregates under physiological conditions and their impact on membranes, providing valuable insights for researchers in this field.

KEYWORDS

Alzheimer's disease, amyloid aggregation, molecular mechanisms, membranes, damage, copper, cholesterol, oxidized

#### 1 Introduction

Amyloid plaques, primarily composed of amyloid beta (AB) peptides, are a key feature of Alzheimer's disease (AD). The detection of Aβ plaques in individuals without the disease prompted the consideration of alternative theories concerning the fundamental cause of AD, such as the cholinergic hypothesis, Aβ oligomer hypothesis, tau hypothesis, mitochondrial cascade hypothesis, calcium homeostasis hypothesis, neurovascular hypothesis, inflammatory hypothesis, metal ion hypothesis, lymphatic system hypothesis, microbial hypothesis, and others (Bagheri et al., 2022; Bagheri et al., 2024; Liu et al., 2019). One of these theories is the "amyloid toxic oligomers hypothesis," which posits that small, soluble AB oligomers are the main source of toxicity, rather than the amyloid plaques themselves (Bagheri et al., 2018). The mechanisms through which Aβ oligomers contribute to the neuropathogenesis associated with AD progression encompass receptor interaction, disruption of cell membranes, impairment of mitochondrial function, dysregulation of calcium homeostasis, and the induction of tau pathology (Huang and Liu, 2020). The effectiveness of medications such as EPPS (Zarrilli et al., 2024) or 8-Hydroxyquinolines (8-HQs) (Ryan et al., 2015), which inhibit the formation of neurotoxic Aβ oligomers by stabilizing smaller, non-toxic aggregates, lends support to the toxic oligomer hypothesis.

Given that A $\beta$  peptides do not typically accumulate under healthy condition and perform numerous physiological functions (Bishop and Robinson, 2004), extensive research has been conducted to understand the reasons and mechanisms behind their accumulation and to answer the question of whether A $\beta$  peptide accumulation is truly the main cause of AD (Bagheri et al., 2018). In the majority of *in vitro* experiments, the A $\beta$  concentration needed is significantly greater than what is typically found in physiological conditions, and no accumulation is detected within the physiological concentration range of A $\beta$  (Lyubchenko, 2020). This article delves into the molecular mechanisms contributing to A $\beta$  accumulation from a biophysical perspective, taking into account the latest scientific advancements.

# 2 Aβ peptides

Aβ is produced via the proteolytic cleavage of the transmembrane protein amyloid precursor protein (APP), a process facilitated by the enzymes  $\beta$ -secretase and  $\gamma$ -secretase (Chen et al., 2017). β-secretase can cleave APP at each of the first 11 residues of the β-site, resulting in the formation of secreted-APP-β and a membrane-associated fragment. Subsequently, y-secretase further cleaves membrane-associated fragment at various sites, leading to the production of AB peptides of varying lengths. The predominant AB peptides generated are 40 amino acids in length; however, peptides with lengths ranging from 38 to 43, and even 46 and 49 amino acids, have been identified in vivo (Zhang et al., 2012). The two predominant alloforms of the peptide are present simultaneously under physiological conditions in the brain, exhibiting an Aβ42:Aβ40 ratio of approximately 1:9. In AD patients, this ratio frequently shifts to a greater proportion of Aβ42, which has a greater tendency to aggregate (Gu and Guo, 2013; Pauwels et al., 2012).

### 2.1 Aβ40

Nuclear magnetic resonance (NMR) diffusion studies show that at 37 °C, soluble A $\beta$ 40 retains its disordered structure and predominantly exists as a monomer, although dimers and other small oligomeric configurations have been observed (Leite et al., 2020). Different oligomer species are in rapid equilibrium, with intensity decreasing as the oligomer size increases (Bitan et al., 2003; Pujol-Pina et al., 2015). A $\beta$ 40 dimers and trimers adopt a globular shape without a well-defined secondary structure (Pujol-Pina et al., 2015).

A study using native ion mobility mass spectrometry and molecular dynamics (MD) simulations discovered that a specific  $\beta$ -hairpin motif in the A $\beta$ 40 peptide sequence is essential for the formation of A $\beta$  oligomers. Initially, the oligomers grow in a spherical manner, but as they exceed tetramers in size, they start to form extended linear aggregates (Khaled et al., 2023).

Conformation-dependent antibodies suggest the existence of at least two fundamentally different categories of amyloid oligomers: fibrillar (FO) and prefibrillar oligomers (PFO) (Glabe, 2008). CD, FTIR, and Raman spectroscopic analyses show that PFOs lack a significant proportion of  $\beta$ -sheets and largely display a disordered

conformation. The denaturation process of PFOs occurs at low concentrations of guanidinium thiocyanate with low cooperativity, suggesting weak intermolecular interactions. A proposed structural model of PFOs suggests that residues 1–25 are disordered, while residues 26–40 are organized into an antiparallel  $\beta$ -barrel (Figure 1). In contrast, A $\beta$ 40 FOs are small aggregates characterized by a high content of  $\beta$ -sheets and exhibit structural similarities to fibrils, albeit with some irregularities in the stacking of  $\beta$ -sheets. However, they demonstrate reduced stability when subjected to denaturation (Breydo et al., 2016).

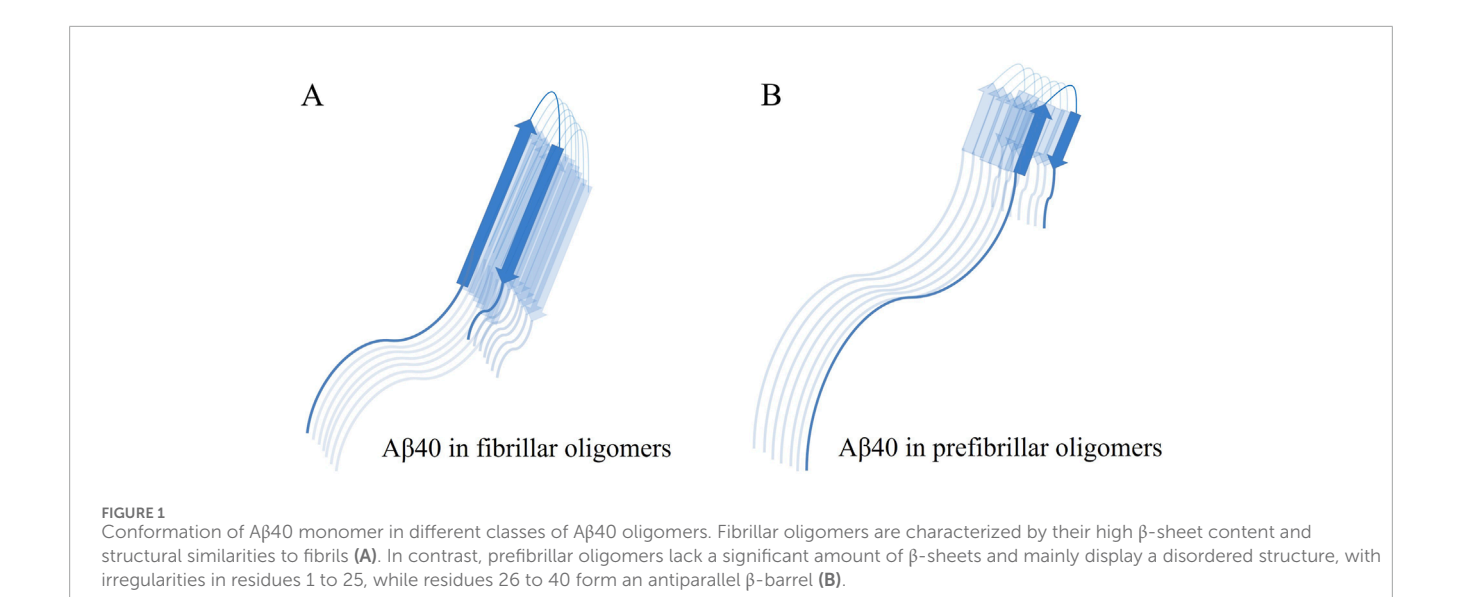
In various oligomeric preparations of numerous amyloidogenic proteins and peptides, annular protofibrils (APFs) have been characterized as ring-shaped or pore-like structures. Their significance lies in the fact that their pore-like structure aligns with multiple studies indicating the membrane-permeabilizing capabilities of amyloid oligomers. It seems that APFs are generated through the circularization of PFO subunits (Kayed et al., 2009).

Experimental observations indicate that high molecular weight oligomers of A $\beta$ 40 (Rh ~ 20 nm) transform into more compact fibril nuclei (Rh ~ 10 nm), while additional fibril nuclei are generated through processes catalyzed by the fibril surface, subsequently leading to the growth of fibrils through the incorporation of soluble A $\beta$  species (Leite et al., 2020). The transient association of A $\beta$ 40 monomers with fibers reveals partially bound conformations, with the most significant interactions observed around the F19-K28 region, while interactions near the C-terminus (L34-G37) are relatively weaker (Brender et al., 2019). Previous research has shown that the gradual interchange between A $\beta$ 40 monomers and fibrils correlates with dynamic interactions occurring at the C-terminus (Kotler, 2015).

A notable characteristic shared by the various fibril structures identified for A $\beta$ 40 is the existence of two  $\beta$ -sheets. The first, known as the N-sheet, includes residues Q15-D23, while the second, referred to as the C-sheet, is composed of residues A30-V36 (Kunnath Muhammedkutty and Zhou, 2025). The predominant polymorph of brain-derived A $\beta$ 40 fibrils found in typical AD patients exhibits completely extended conformations for the molecules in the central two cross- $\beta$  layers, with  $\beta$ -hairpin conformations observed for the molecules in the outer cross- $\beta$  layers (Ghosh et al., 2021). The intermolecular interaction between Gly25 and Ile31 prevents the typical hairpin configuration seen in A $\beta$ 40 fibrils, promoting the extended conformation in these specific monomers (Scheidt et al., 2024).

#### 2.2 Aβ42

A $\beta$ 42 monomers consist of various ordered and disordered conformational species (Zhuang et al., 2010). Although A $\beta$ 42 and A $\beta$ 40 share the same amino acid sequence with the exception of two extra C-terminal residues, A $\beta$ 42 exhibits a greater tendency to aggregate compared to A $\beta$ 40 (Mamone et al., 2021). The C-terminus of A $\beta$ 42 has greater structural integrity compared to A $\beta$ 40, with the development of a  $\beta$ -hairpin within the sequence 31–42, leading to decreased flexibility and increased fibril formation (Sgourakis et al., 2007). The free energy landscape of amyloid nucleation shows that the C-terminus (residues 29–42) of A $\beta$ 42 is crucial in the rate-limiting step of nucleation (Arutyunyan et al., 2025). The



dynamic behavior of the C-terminal residues in A $\beta$ 42 affects the backbone dynamics of residues V24 to K28 (Mamone et al., 2021). The A $\beta$ 42 monomer often assumes conformations in which the N-terminus region is structured in a manner closely resembling its configuration within the fibril. This inherent tendency of the monomeric A $\beta$  to take on fibril-like conformations may account for the minimal free energy barrier associated with the elongation of A $\beta$ 42 fibrils (Barz et al., 2021). Findings from *in situ* atomic force microscopy (AFM) show that the typical growth rates of A $\beta$ 42 fibrils are approximately 50 times quicker than those of A $\beta$ 40 fibrils (Sunil Menon et al., 2025).

Electrospray ionization ion mobility mass spectrometry (ESI-IM-MS) analysis reveals that Aβ42 primarily oligomerizes into dimers and trimers, which take on a spherical form and do not exhibit a clear secondary structure (Pujol-Pina et al., 2015). ESI-IMS-MS is an analytical technique that is advancing swiftly for the analysis of intricate compounds in the gas phase. ESI-IMS-MS effectively separates isomers, offers structural insights, and quantitatively identifies peptides, lipids, carbohydrates, polymers, and metabolites found in biological samples (Kohoutek and Harrington, 2023). Transmission electron microscopy and atomic force microscopy (AFM) data analysis showed that round particles, averaging 10-15 nm in width, were more toxic than fibrils and protofibrils. Size exclusion chromatography indicated a single size distribution of 24 ± 3 kDa for the oligomer samples, suggesting a pentameric structure. These oligomers lack the  $\beta$ -sheet structure present in fibrils and instead consist of loosely aggregated strands with protected C termini and a turn conformation, facilitating interaction between Phe19 and Leu34 (Ahmed et al., 2010). Unlike fibrils, the  $\beta$ -strands in oligomers are not arranged in in-register parallel  $\beta$ -sheets. This unique arrangement of  $\beta$ -strands may act as an energy barrier, impeding the transformation of oligomers into fibrils or the initiation of monomer conversion into fibrils (Tay et al., 2013).

The 3D structure of a disease-associated A $\beta$ 42 fibril polymorph, determined through the integration of solid-state NMR spectroscopy data and mass-per-length assessments from electron microscopy, reveals the presence of two molecules within each

fibril layer. This structure is defined by residues 15–42, forming a double-horseshoe-like cross- $\beta$ -sheet configuration that effectively hides hydrophobic side chains. In contrast, residues 1–14 show partial ordering and adopt a  $\beta$ -strand conformation (Wälti et al., 2016). Studies on A $\beta$ 42 fibrils, whether synthesized *in vitro* or extracted from brain tissue, have identified polymorphs with variations in amino acid side chain orientations, structurally ordered segment lengths, and interactions between cross- $\beta$  subunit pairs within a single filament, while maintaining a common S-shaped configuration for individual A $\beta$ 42 molecules. In contrast, fibrils generated through seed growth, using tissue fibrils as seeds, exhibit distinct structural features. These structures qualitatively differ in various aspects, displaying molecular configurations resembling the Greek letters  $\nu$  and  $\nu$  rather than the letter  $\nu$  (Lee et al., 2023).

The application of high-speed AFM technique revealed two distinct morphomers, "straight" and "spiral," formed during Aβ42 fibril aggregation. Each growth mode is contingent upon the structure of the initial fibril nucleus; however, transitions from one growth mode to another are sometimes detected. This indicates that the structure at the end of the fibril oscillates between the two growth modes and is indeed influenced by relatively minor alterations in environmental conditions (Watanabe-Nakayama et al., 2016). In situ AFM imaging identified two distinct aggregation pathways that do not cross: one leading to amyloid fibrils and the other to oligomers and amorphous aggregates (Sunil Menon et al., 2025). ThT analysis and high-speed AFM observations showed that globular-shaped Aβ oligomers (gABO) facilitated the fibril formation of low molecular weight Aβ42 (including dimers, trimers, and oligomers with fewer than 8 monomers), whereas gABO itself did not lead to the formation of fibrous aggregates (Nakano et al., 2025).

### 3 Amyloid content of plaques

In the brain of patients with sporadic AD (SAD), amyloid plaques are mainly composed of A $\beta$ 42, with some plaques containing only A $\beta$ 42, despite the higher concentration of A $\beta$ 40

(Gu and Guo, 2013; Tehrani et al., 2024). Previous studies have shown that diffuse plaques in SAD brains are exclusively positive for A $\beta$ 42 and negative for A $\beta$ 40. In contrast, in the cortices of elderly people not living with dementia, senile plaques often exhibit strong positivity for A $\beta$ 40 (Iwatsubo et al., 1994).

Analysis of cortical specimens from familial AD (FAD) patients with the APP717 (Val to Ile) mutation revealed a high prevalence of plaques positive for A $\beta$ 42 and negative for A $\beta$ 40 (Iwatsubo et al., 1994). In contrast, FAD patients with the Arctic (E22G) mutation in A $\beta$  exhibit a higher A $\beta$ 40 concentration in the core of amyloid plaques. Cotton-wool plaques, large spherical structures up to approximately 120  $\mu$ m in diameter, larger than the typical 10  $\mu$ m diameter of amyloid plaques in sporadic AD, are more common in Arctic FAD cases (Tehrani et al., 2024). High-resolution cryoelectron microscopy analysis of A $\beta$  filaments extracted from the frontal cortex of an individual with the Arctic mutation revealed that the predominant filaments consist of two distinct pairs of protofilaments: residues V12-V40 (human Arctic fold A) and E11-G37 (human Arctic fold B) (Yang et al., 2023).

Reduced levels of insoluble A $\beta$ 42 were observed in the frontal and temporal cortex of APPsw mutation carriers. In contrast, presenilin-1 (PS1) mutation carriers showed significantly lower levels of both insoluble A $\beta$ 40 and A $\beta$ 42 in all four cortical regions compared to those with SAD. Additionally, individuals with the PS1 mutation exhibited a notably elevated ratio of insoluble A $\beta$ 42 to A $\beta$ 40 (Hellström-Lindahl et al., 2009). PS1 acts as the catalytic component of  $\gamma$ -secretase, an intramembranous protease responsible for cleaving APP. Notably, mutations in the PSEN1 gene, encoding PS1, represent the predominant cause of FAD (Kelleher and Shen, 2017).

# 4 Differences between A $\beta$ 40 and A $\beta$ 42 in gathering

The aggregate-free A $\beta$ 40 exists in the forms of monomers, dimers, trimers, and tetramers, maintaining a rapid equilibrium state. In contrast, A $\beta$ 42 tends to preferentially form pentamer and hexamer units, known as paranuclei, which then assemble into beaded superstructures resembling early protofibrils (Bitan et al., 2003). However, some studies suggest that the presence of A $\beta$ 42 pentamers and hexamers may be an experimental artifact; highlighting that A $\beta$ 42 oligomerization primarily occurs through dimers and trimers (Pujol-Pina et al., 2015). Furthermore, high-resolution studies of fibril-like interactions in spherical oligomers of A $\beta$ 40 have shown the presence of parallel  $\beta$ -sheets, while A $\beta$ 42 oligomers lack  $\beta$ -sheet secondary structure, indicating significant differences in the structural characteristics and toxicity of these A $\beta$  forms (Kotler, 2015).

Minor modifications in the A $\beta$ 42/A $\beta$ 40 ratio have a significant impact on the biophysical and biological characteristics of A $\beta$  mixtures, affecting their aggregation kinetics, the structure of resulting amyloid fibrils, and synaptic functionality both *in vitro* and *in vivo*. A slight increase in the A $\beta$ 42/A $\beta$ 40 ratio promotes the stabilization of toxic oligomeric forms with intermediate conformations. Initially, these A $\beta$  species have detrimental effects on synapses, leading to toxicity that can spread within cells and ultimately result in neuronal cell death. There is a dynamic balance

between toxic and non-toxic intermediates (Kuperstein et al., 2010). Studies have shown that the oligomers formed in the peptide mixture solution are predominantly co-oligomers, especially at the physiological A $\beta$ 42 to A $\beta$ 40 ratio (1:10), underscoring the significant influence of A $\beta$ 40 on oligomer formation and aggregation processes (Meng et al., 2024). While both A $\beta$ 40 and A $\beta$ 42 initially produce larger oligomers on neurites compared to glass slides, a 1:1 combination of these peptides result in the formation of smaller oligomers attached to neurites than those observed on slides or with either peptide alone. At physiological concentrations, small A $\beta$ 0 oligomers adhere to the membrane and gradually increase in size over time, with the kinetics of this process being influenced by the local ratio of A $\beta$ 42 to A $\beta$ 40 (Johnson et al., 2013).

Protofibrils formed from a combination of A $\beta$ 42 and A $\beta$ 40 are mainly composed of A $\beta$ 42, with minimal incorporation of A $\beta$ 40. However, even in small amounts, A $\beta$ 40 can influence the structural characteristics of A $\beta$ 42 protofibrils (Terrill-Usery et al., 2016). An increase in the A $\beta$ 42/A $\beta$ 40 ratio promotes protofibril formation; however, the inclusion of A $\beta$ 40 in mixed A $\beta$  solutions significantly hinders this process. When the A $\beta$ 42/A $\beta$ 40 ratio is elevated, the size of protofibrils remains relatively constant, while the  $\beta$ -sheet structure is strengthened (Terrill-Usery et al., 2016).

Monomeric A $\beta$ 40 significantly affects the kinetic stability, solubility, and morphological features of A $\beta$ 42 aggregates, hindering their conversion into mature fibrils. When present in approximately equimolar concentrations (A $\beta$ 40/A $\beta$ 42 around 0.5–1), A $\beta$ 40 can inhibit over 50% of fibril formation initiated by monomeric A $\beta$ 42. Moreover, the inhibition of protofibrillar A $\beta$ 42 fibrillogenesis occurs at lower, substoichiometric ratios (A $\beta$ 40/A $\beta$ 42 approximately 0.1) (Jan et al., 2008). Recent studies also indicate that A $\beta$ 42 aggregation is decelerated by A $\beta$ 40, while A $\beta$ 40 aggregation is accelerated by A $\beta$ 42 in a concentration-dependent manner (Meng et al., 2024).

The Aβ42 fibril is characterized by a single protofilament, whereas the Aβ40 fibril consists of two protofilaments. The threedimensional configuration of the Aβ42 protofilament is composed of two superimposed, intermolecular, parallel, in-register β-sheets that extend along the axis of the fibril (Lührs et al., 2005). Research employing high-speed AFM to examine the growth process of fibrils indicates that Aβ42 molecules are added alternately to each of the two cross- $\beta$  subunits within the protofilament (Yagi-Utsumi et al., 2024). Both Aβ42 and Aβ40 fibrils exhibit axial twofold symmetry and have similar protofilament structures. Additionally, the protofilaments of both Aβ40 and Aβ42 fibrils contain the same number of Aβ molecules within each cross-β repeat (Schmidt et al., 2009). Although the fibrillogenesis of both monomeric forms can be initiated by fibrils derived from either peptide, it is the Aβ42 protofibrils that specifically facilitate the fibrillogenesis of monomeric A $\beta$ 42, while leaving monomeric A $\beta$ 40 unaffected (Jan et al., 2008). Solid-state NMR studies have shown that the C-terminal Ala42, unique to Aβ42, forms a salt bridge with Lys28, serving as a molecular switch for self-recognition and excluding A $\beta$ 40 from the process (Xiao et al., 2015).

#### 5 Post-translational modifications

The composition of  $A\beta$  in the brains of AD patients was analyzed to investigate potential associations between post-translational

modifications and the accumulation of this peptide in affected tissues (Roher et al., 1993). Studies have shown that, in addition to the well-known A $\beta$ 40/42 variants, A $\beta$  peptides extracted from the brains of AD patients and amyloid plaque cores exhibit truncated N- and C-termini, as well as other post-translational modifications (Kumar et al., 2020; Roher et al., 2017).

The peptide compositions in the cerebrovascular and senile plaque core amyloid deposits of AD patients show significant variability in the amino-terminal region, with a diverse array of peptides starting with each of the initial eleven amino acids in the A $\beta$  sequence and ending with Ala42 (Miller et al., 1993). A physiologically relevant variant of truncated A $\beta$  is generated through initial truncation at the N-terminus at a glutamic acid residue (E3 or E11), which is then cyclized into a pyroglutamate form (pE3 or pE11). Both variants have been detected in elevated levels within the amyloid plaque cores (Scheidt et al., 2024).

The structural characteristics of oligomers and fibrils formed by the peptides pE3-A $\beta$ 3-40 and pE11-A $\beta$ 11-40 closely resemble those of wild-type A $\beta$ 40 (Scheidt et al., 2016; Scheidt et al., 2020; Scheidt et al., 2017). However, pE3-A $\beta$ 3-40 shows a higher tendency to adopt  $\beta$ -sheet-dominant structures and form large fibrils in the presence of a helix-stabilizing co-solvent (trifluoroethanol), while wild-type A $\beta$ 40 mainly adopts  $\alpha$ -helical structures and lacks ThT-positive structures (Dammers et al., 2015). Studies have also suggested that pE11-A $\beta$ 11-40 fibrils exhibit greater toxicity compared to wild type A $\beta$ 40 and pE3-A $\beta$ 3-40 (Scheidt et al., 2017).

Among the truncated N-terminal isoforms, the pE3-A $\beta$ 3-42 isoform is the predominant variant, showing a higher  $\beta$ -sheet content and increased aggregation compared to monomeric A $\beta$ 42 (Dammers et al., 2017; Nath et al., 2023). This characteristic results in the formation of large fibrils that can be visualized through electron microscopy, a feature absent in A $\beta$ 42. Initially, when dissolved, pE3-A $\beta$ 3-42 displays two  $\alpha$ -helical regions linked by a flexible linker, while the N-terminus remains disordered. Studies suggest that these  $\alpha$ -helices act as a transient intermediate stage in the transition to  $\beta$ -sheet and fibril formation of pE3-A $\beta$ 3-42 (Dammers et al., 2017). The pE3-A $\beta$ 3-42 fibrils exhibit similar positions of  $\beta$ -strands and maintain a conserved turn region surrounding V24, resembling the LS-shaped fibrils of A $\beta$ 42 (Gardon et al., 2024).

Phosphorylation of the serine-8 residue (pS8) in A $\beta$ 40 facilitates the formation of oligomeric A $\beta$  aggregates, which act as nuclei for fibrillization. This modification increases toxicity, enhances aggregation, accelerates the process, and eliminates the lag phase in aggregation process. Moreover, phosphorylation at serine-8 encourages the development of  $\beta$ -sheet structures (Bagheri and Saboury, 2022; Kumar et al., 2011). The structural characteristics of the N-terminal region in pS8-A $\beta$ 40 fibrils display significant differences compared to all previously identified wild-type A $\beta$ 40 fibrils, showing strong intra-strand interactions that promote close association between the N terminus and the amyloid core (Hu et al., 2019).

Phosphorylation of serine-8 in  $A\beta42$  enhances  $\beta$ -sheet formation, accelerating amyloid aggregation in a synthetic lipid environment. This modification increases cellular binding affinity and reduces neurotoxic effects (Jamasbi et al., 2017). Despite pS8-A $\beta42$  aggregating faster than A $\beta42$ , zinc ions inhibit its aggregation. Phosphorylation of A $\beta$  at serine-8, located in the zinc-binding

domain, significantly alters zinc-induced oligomerization. Zinc-induced oligomerization of A $\beta$  may serve as a seeding mechanism for neurotoxic A $\beta$  oligomers and aggregates (Barykin et al., 2018).

An additional modification that occurs significantly more frequently in brain samples from AD patients than in healthy controls is  $A\beta$  isomerization. For instance, the  $A\beta$ 1-15 species exhibits around 85% isomerization in insoluble plaques and membrane fractions from the brain samples of patients, while control samples show only 50% (Mukherjee et al., 2021).

The isoAsp7-Aβ variant is the predominant form found in pathological conditions, with Aβ4-X, pGlu3-Aβ, pGlu11-Aβ, and pS8-Aß following in abundance (Schrempel et al., 2024). Another study suggests that the accumulation of isoD-A\beta starts with aging, while the deposition of pE3-Aβ is more directly linked to AD (Moro et al., 2018). The aggregation of A $\beta$  can be divided into three distinct biochemical stages, characterized by the presence of pE3-Aβ and phosphorylated Aβ in a hierarchical manner. Western blot analysis revealed that in the initial preclinical phase of AD (biochemical stage 1 of Aβ aggregation), various forms of AB aggregates—soluble, dispersible, membrane-associated, and plaque-associated-showed no detectable levels of pE3-Aβ or phosphorylated Aβ. In the subsequent biochemical stage 2, pE3-Aβ was detected, while phosphorylated Aβ was exclusively observed in the final stage of AB aggregation, which is biochemical stage 3 (Rijal Upadhaya et al., 2014).

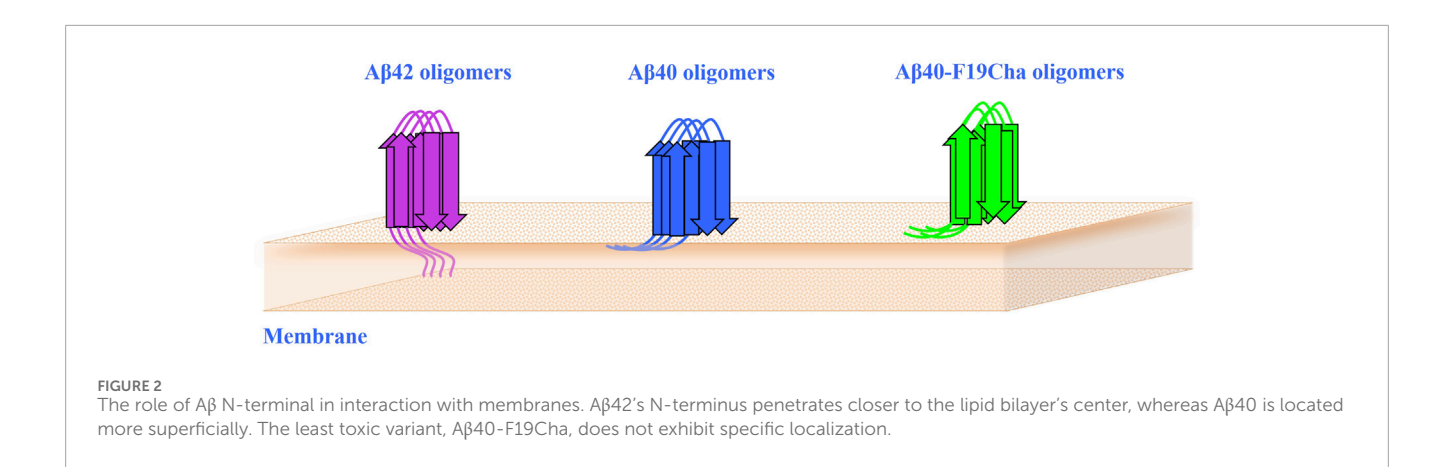
In the aggregation assay, isoAsp7-A $\beta$ , pGlu3-A $\beta$ , and pGlu11-A $\beta$  variants showed rapid fibril formation without any delay, while the other variants, which were absent in plaque formations, such as isoAsp27-A $\beta$ , did not exhibit fibril formation (Schrempel et al., 2024). N-terminally modified A $\beta$  variants such as pS8-A $\beta$ 40, Y10-nitrated A $\beta$ 40 (nY10-A $\beta$ 40), and isoAsp7-A $\beta$ 40 alter the structural properties and cytotoxicity of wild-type A $\beta$  fibrils through cross-seeding (Hu et al., 2020). For instance, pS8-A $\beta$ 40 fibrils can cross-seed with wild-type A $\beta$ 40 monomers, resulting in more stable and rigid fibrillar structures compared to self-nucleated wild-type A $\beta$ 40 fibrils (Hu et al., 2019).

IsoAsp7-A $\beta$ 42 and pS8-A $\beta$ 42 isoforms have shown enhanced ability to cross the blood-brain barrier compared to unmodified A $\beta$ 42, attributed to distinct endocytosis mechanisms influencing their transport. The lower binding affinity of pS8-A $\beta$ 42 and isoAsp7-A $\beta$ 42 for RAGE compared to A $\beta$ 42 may reduce their intracellular accumulation, facilitating more effective translocation to the abluminal side (Varshavskaya et al., 2024).

# 6 Role of membranes in $A\beta$ aggregation

In vitro aggregation studies typically use A $\beta$  concentrations in the micromolar range. However, the physiological levels of A $\beta$  in the brain are in the low nanomolar range, suggesting that spontaneous aggregation of A $\beta$  peptides is unlikely under these conditions (Lyubchenko, 2023). Nonetheless, further research has shown that the spontaneous formation of A $\beta$  oligomers can occur at physiologically relevant concentration. This phenomenon is attributed to a surface aggregation mechanism where the surface acts as a catalyst for aggregation (Lyubchenko, 2020).

frontiersin.org



### 6.1 Aβ42 aggregation

At nanomolar concentrations, Aβ42 shows a strong preference for surface aggregation over bulk solution pathways (Banerjee et al., 2017). MD simulations indicate that when a monomer interacts with the surface, it undergoes a conformational change. Subsequent binding of another monomer to this altered form leads to the formation of a dimer, causing both monomers to undergo conformational shifts. This surface interaction facilitates the rapid formation of dimers (Banerjee et al., 2017). Energy landscapes of AB42 dimerization reveal that disordered states have the lowest energy for Aβ42 monomers, while the lowest energy minima for dimers consist of more ordered structures, primarily βhairpins. These structures form as Aβ42 folds upon binding to the hydrophobic region of another Aβ42 peptide (Schäffler et al., 2024). Recent experimental studies have shown that the proportion of  $\beta$ -sheets in  $A\beta$  increases threefold upon initial interaction with the membrane (Heermant et al., 2025).

Distinct differences exist in the interaction behaviours of A $\beta$ 42 and A $\beta$ 40 monomers when they form dimers. Although the sequence variation between these peptides lies in the C-termini, it is the N-terminal segment that significantly influences their interactions within dimers. The N-terminal region of the A $\beta$ 40 peptide contributes to reduced interpeptide interactions, but the additional two residues in A $\beta$ 42 counteract this effect (Lv et al., 2013). Furthermore, the N-terminal regions of A $\beta$ 42 dimers play a role in A $\beta$  aggregation within membrane environments (Press-Sandler and Miller, 2022). Findings from a single molecule technique (QSLIP) suggest that the N-terminus of A $\beta$ 42 penetrates near the core of the lipid bilayer, while the less harmful A $\beta$ 40 is located at a shallower level (Figure 2). The least toxic variant, A $\beta$ 40-F19Cha, does not exhibit distinct localization (Dey et al., 2024).

Membranes with low packing density promote A $\beta$ 42 fibrillation, resulting in shorter fibrils compared to membranes with high packing density. The presence of cis-double bonds in lipid acyl chains reduces packing density, enhancing hydrophobic interactions with A $\beta$ 42. Conversely, anionic lipids inhibit A $\beta$ 42 fibrillation by establishing strong electrostatic interactions that tightly bind A $\beta$ 42 to the membrane surface (Heo et al., 2021). Despite A $\beta$ 's negative charge at physiological pH, studies show that A $\beta$  can interact with anionic lipids through electrostatic forces, involving interactions

between positively charged peptide residues and negatively charged lipid head groups (Bokvist et al., 2004; Niu et al., 2018).

Analysis of biomimetic membranes mimicking cellular oxidative stress, compared to mammalian and bacterial membranes, revealed that incorporating oxidized lipids as a cellular stress mimic had effects on peptide self-assembly similar to bacterial mimetic membranes. Electrostatic interactions were found to be crucial in facilitating peptide-membrane binding (John et al., 2023).

All-atom MD simulations have shown that the A $\beta$ 42 dodecamer has a more pronounced disruptive effect on neuronal membranes compared to the mature fibril. The study highlights the significance of electrostatic interactions between A $\beta$  and the membrane, with these interactions playing a more crucial role than van der Waals interactions. Additionally, the electrostatic interaction energy associated with fibrils is stronger than that of the dodecamer. The interaction between A $\beta$  and the membrane is mainly influenced by repulsive electrostatic forces between A $\beta$  and the ganglioside GM1 lipid. Importantly, the A $\beta$ 42 dodecamer can approach the membrane more closely than the fibril (Nguyen et al., 2022).

MD simulations investigating the impact of cholesterol on the binding of fibrils to lipid bilayers have revealed that  $A\beta$  fibrils exhibit a higher affinity for bilayers with elevated cholesterol concentrations. The binding interactions are predominantly governed by electrostatic forces, leading to longer lifetimes and increased binding frequency as cholesterol levels increase (Dias et al., 2020).

#### 6.2 Aβ40 aggregation

The CD spectrum of unbound A $\beta$ 40 indicates a random coil structure (Figure 3). A $\beta$ 40 monomers do not immediately change their conformation upon interacting with membranes, remaining mostly unfolded with some minor conformations. However, as fibrillation commences, A $\beta$ 40 progressively transitions from its native random coil structure to a  $\beta$ -sheet conformation (Bera et al., 2020).

Experiments using fluorescence and Raman spectroscopy on membrane-bound A $\beta$ 40 oligomers have shown that these structures adopt an antiparallel  $\beta$ -sheet conformation, with the C-terminus more deeply embedded than the N-terminus (Bhowmik et al., 2015; Chandra et al., 2018). The integration of A $\beta$ 40 into membrane structures promotes the shift from antiparallel to parallel  $\beta$ -sheet

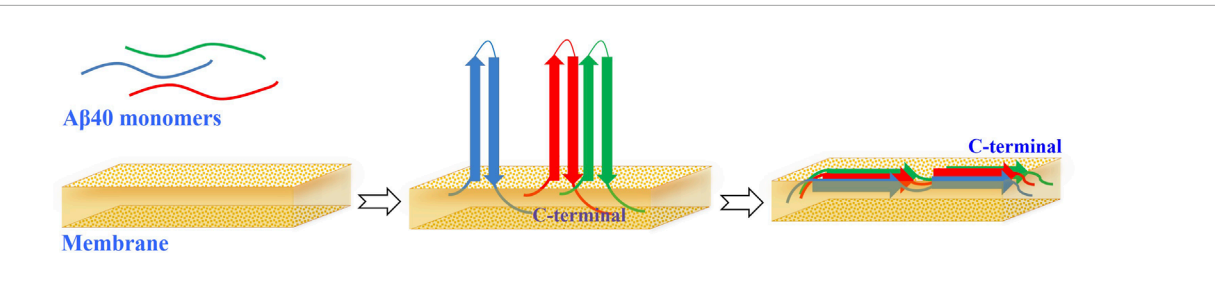


**FIGURE 3**A $\beta$ 40 changes in the presence of membranes. When unbound, A $\beta$ 40 adopts a random coil configuration. However, when bound to membranes, A $\beta$ 40 oligomers form an antiparallel  $\beta$ -sheet structure, with the C-terminus positioned deeper than the N-terminus. The integration of A $\beta$ 40 into membrane promotes the transition from antiparallel to parallel  $\beta$ -sheet arrangements.

configurations (Figure 3), which occurs abruptly after a delay, indicating a cooperative mechanism at play (Heermant et al., 2025). This transition is influenced by the charge of the lipids, with negatively charged membrane interfaces amplifying the observed effects. In contrast,  $A\beta$  behaves similarly in the presence of neutral lipids, but to a lesser extent. Notably, in positively charged lipid membranes, there are no detectable amide I signals characteristic of  $\beta$ -sheets (Heermant et al., 2025).

Various membrane compositions have been shown to enhance the aggregation kinetics of A $\beta$ 40, accompanied by distinct transitions in the peptide's secondary structure. The core and C-terminal residues primarily influence the interactions between A $\beta$ 40 and the membrane. These conformers of A $\beta$ 40, which exhibit structural differences, are morphologically and functionally different from A $\beta$ 40 that lacks lipid components (Bera et al., 2020). MD simulations indicate that the secondary structure of the C-sheet remains largely intact within the membrane, whereas the N-sheet exhibits fraying at its ends. After the formation of a small oligomeric seed within the membranes, it is subsequently released into the surrounding aqueous environment. The residue Y10 serves to anchor the N-sheet to the membranes, while the C-sheet is liberated (Kunnath Muhammedkutty and Zhou, 2025).

## 7 Membrane damage

At low nanomolar concentrations, A $\beta$ 42 has been shown to have no harmful effects on supported lipid bilayers (van Deventer and Lyubchenko, 2024). Previous studies using FRET microscopy have similarly indicated that the membrane model remains mostly intact at a concentration of 100 nM A $\beta$  (Chandra et al., 2018). Additionally, initial experiments on calcium leakage showed that treatment with A $\beta$  at concentrations below 10 nM did not lead to significant toxicity compared to the control group (Johnson et al., 2013). This raises questions about the mechanisms through which A $\beta$  may cause membrane damage.

At concentrations below 10 nM, monomers consistently bind to the membrane surface without forming oligomers or disrupting the membrane. As the concentration increases from 10 nM to several hundred nanomolar, monomers continue to bind uniformly while dimers and small oligomers start to appear. Dimers do not cause membrane permeabilization, but larger oligomers can

induce permeabilization, with each oligomer contributing to ion conductance of less than 10 pS per pore (Schauerte et al., 2010).

The disruption of membranes is associated with amyloid species that exist as transient small oligomeric entities during the initial phases of aggregation, characterized by morphologies comprising small globular species measuring less than 10 nm in diameter (Feuillie et al., 2020). Additionally, other research indicates that the detrimental effects of Aβ42, with an average diameter of 5.2 nm, are significantly more pronounced than those associated with the smaller 3.9 nm species (Yasumoto et al., 2019). Moreover, large soluble oligomers of Aβ (≥150 kDa) from AD brains are much less toxic than the smaller oligomers (~8-70 kDa) they break down into (Yang et al., 2017). AFM imaging revealed that A $\beta$  deposits gradually separated from the membrane, leading to the excision of portions of the underlying bilayer (Azouz et al., 2019). Furthermore, time-lapse AFM imaging in solution demonstrates that, as time progresses, both the size and number of oligomers increase while they are released into the solution. This finding suggests that the aggregates formed could serve as nucleation sites, promoting additional aggregation within the surrounding solution (Banerjee et al., 2017).

Aβ42 oligomers have a greater tendency to infiltrate and create perforations in the membrane, unlike monomers, which only adhere to the membrane's exterior without the ability to penetrate its structure (Figure 4) (Nag et al., 2013; Robinson et al., 2025; Sarkar et al., 2013). Furthermore, Aβ42 oligomers exhibit significant cytotoxic effects and are easily internalized by neurons, whereas Aβ42 fibrils show reduced internalization and lack any toxic effects. Additionally, sonication of Aβ42 fibrils produces species similar in size to oligomers, yet these remain nontoxic. Therefore, it is clear that Aβ42 oligomers possess distinct characteristics that contribute to their neurotoxic capabilities (Vadukul et al., 2020). The greater bilayer perturbations caused by G37C oligomers compared to Aβ42 confirm this observation, suggesting that oligomers unable to progress to the fibril state can exhibit significant toxicity (Azouz et al., 2019).

Numerous studies using AFM methods, electrophysiology, and cell biology have shown that A $\beta$  can induce pore-like structures and stimulate channel activity in membranes (Connelly et al., 2012; Demuro et al., 2011; Lal et al., 2007; Quist et al., 2005). Membrane patches from HEK293 cells were used to investigate the channel-forming abilities of monomeric, oligomeric, and fibrillar forms of A $\beta$ 40 and A $\beta$ 42 in a more physiological context. The results revealed that A $\beta$ 42 oligomers form voltage-independent, non-selective ion

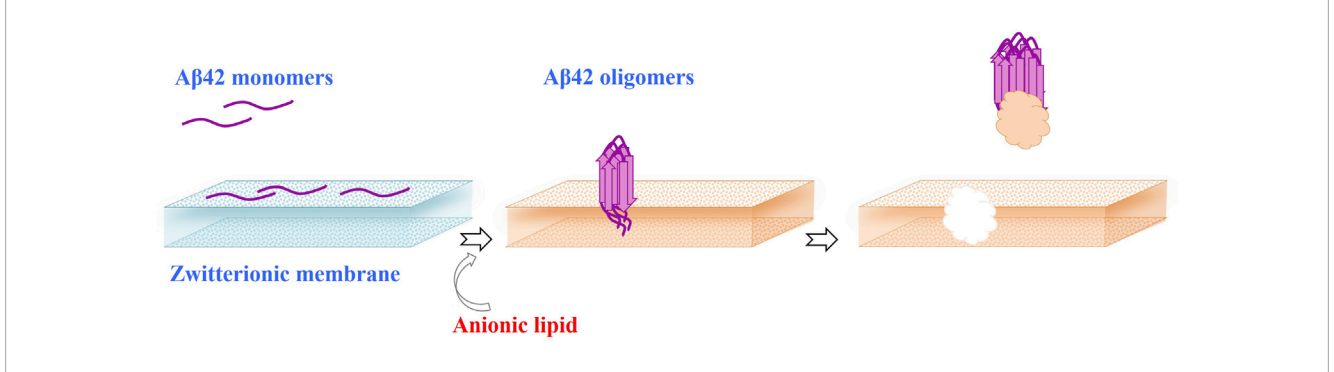


FIGURE 4
Interaction of A $\beta$ 42 with membrane. A $\beta$ 42 oligomers exhibit a higher propensity to penetrate the membrane and form pores, in contrast to monomers that simply bind to the outer surface of the membrane without penetrating it. A $\beta$ 42 monomers show limited adsorption to zwitterionic membranes, failing to form aggregates. However, the presence of anionic phospholipids in the membrane induces the oligomerization of A $\beta$ 42 monomers, leading to membrane disruption.

channels, while  $A\beta40$  oligomers, fibers, and monomers do not exhibit channel formation (Bode et al., 2017). A minimum of six monomeric subunits of  $A\beta40$  oligomers is required to induce significant conductance in model membranes, but the levels of these oligomeric structures were found to be minimal, suggesting minor effects on neuronal function (Johnson et al., 2013).

High-speed AFM studies showed that stable oligomeric species like Aβ42-oG37C, which do not fibrillate, do not interact with membranes composed of phosphatidylcholine and sphingomyelin. The presence of ganglioside GM1 is crucial for the peptide's interaction with the membrane, facilitating its insertion through nearby cholesterol and leading to membrane disruption (Ewald et al., 2019). Simulations highlighted the roles of GM1 and cholesterol in stabilizing membrane-embedded β-sheets, as well as functions of Y10 and K28 in releasing small oligomeric seeds into the solution (Kunnath Muhammedkutty and Zhou, 2025). MD simulations have shown that sphingomyelin, unlike GM1, promotes a  $\beta$ -sheet-rich conformation in A $\beta$ 42 monomers at physiologically relevant concentrations. The increased rigidity of the bilayer due to sphingomyelin reduces interactions with the N-terminus of Aβ42, inhibiting its embedding and promoting a βsheet structure in the N-terminal region, resembling higher-order Aβ fibrils (Owen et al., 2018).

Calorimetric investigations revealed that Aβ42 fibrils, oligomers, and monomers can bind to or integrate into bilayers in a liquid-ordered state, regardless of their electric charge. However, monomers do not interact with electrically neutral bilayers (Ahyayauch et al., 2024). The key factor influencing the aggregation process is the affinity of  $A\beta$  monomers for the membrane surface, rather than the concentration of Aβ (Lyubchenko, 2020). Monomeric Aβ42 weakly adsorbs to zwitterionic DOPC membranes without forming aggregates. However, the addition of 10 mol% DOPS (anionic phospholipids) to the outer leaflet of the membrane induces the oligomerization of Aβ42 monomers (Figure 4), leading to membrane damage (Robinson et al., 2023). AFM results suggest that the inclusion of cholesterol or GM1 at a concentration of 10 mol% in zwitterionic POPC membranes promotes the formation of a liquid-disordered-phase domain, facilitating Aβ42 aggregation and causing membrane fragmentation (Azouz et al., 2019).

Studies on POPC membranes with cholesterol or GM1 have shown that A $\beta$ 42 induces the formation of small aggregates on cholesterol-containing membranes, measuring several nanometers, and small fibers on GM1-containing membranes, approximately 10 nm in height. Detachment of these deposits from POPC membranes with cholesterol creates perforations in the outer layer, while detachment from POPC membranes with GM1 results in holes within the bilayer (Azouz et al., 2019). Additionally, membrane thickness plays a significant role in the morphological changes upon A $\beta$ 40 adsorption. Thicker DOPC and POPC supported lipid bilayers undergo remodeling, forming elongated tubules and globular structures to alleviate membrane stress in response to varying A $\beta$ 40 concentrations. In contrast, thin DLPC membranes do not undergo significant membrane remodeling (Meker et al., 2018).

### 8 Membrane changes in AD and aging

Numerous studies have shown that Aβ, when externally introduced, selectively binds to specific cells within a seemingly uniform cell population in culture. The binding affinity of Aβ to cellular membranes is significantly influenced by the presence of specific lipid constituents like cholesterol, sphingolipids, gangliosides, and various phospholipids (Burke et al., 2013). The structure of cellular membranes undergoes changes with aging and in AD (Drolle et al., 2017). Analysis of the lipid composition of lipid rafts from both control and early-stage AD subjects suggests that lipid composition modifications within cortical lipid rafts occur early in sporadic AD, facilitating interactions between APP and BACE1. These lipid changes in AD lipid rafts result in increased membrane order and viscosity in these regions (Fabelo et al., 2014). Research utilizing various techniques, has shown that multicomponent lipid models, mimicking both healthy and pathological neuronal membrane states, exhibit distinct variations in their nanoscale architecture and physical properties. Moreover, these models demonstrate different interactions with Aβ42, indicating that those representing diseased membranes are more prone to interactions with A\beta and its detrimental effects (Drolle et al., 2017).

# 9 Role of copper in $A\beta$ accumulation and membrane damage

Copper significantly influences the aggregation of A $\beta$ 42, enhancing its cytotoxicity while having minimal impact on A $\beta$ 40. This is attributed to the strong interactions between copper and A $\beta$ 42, leading to conformational changes and stabilization of toxic nanoscale oligomers, unlike the effect on A $\beta$ 40 (Bagheri et al., 2022; Jin et al., 2011). The Arctic variant of A $\beta$ 40 exhibits unique behavior compared to wild-type A $\beta$ 40, as substoichiometric copper concentrations can induce the formation of toxic oligomers similar to those formed with wild-type A $\beta$ 42 (Tian et al., 2024). Copper also affects the assembly of A $\beta$ 40 and A $\beta$ 42 differently, promoting fibril formation of A $\beta$ 40 by enhancing primary nucleation, while stabilizing A $\beta$ 42 as prefibrillar oligomers and protofibrils. Notably, the introduction of copper to pre-existing A $\beta$ 42 fibrils leads to their disassembly, reverting them to protofibrils and oligomers (Tian et al., 2024).

Furthermore, copper overload leads to increased cholesterol synthesis through ROS-dependent and independent pathways, elevating cholesterol levels in cell membranes and lipid rafts. Despite unchanged total APP levels, its presence in lipid rafts increases during copper overload, correlating with higher A $\beta$  concentrations in the culture medium (Bagheri et al., 2018; Zubillaga et al., 2022).

# 10 Concluding remarks

This article aims to explore the differences in the accumulation of A $\beta$ 40 and A $\beta$ 42 from a biophysical perspective, drawing on recent scientific advancements. It also discusses the detrimental effects these amyloids can have on membranes, providing a comprehensive overview for readers interested in this topic.

In summary, despite differing in only two amino acids, A $\beta$ 40 and A $\beta$ 42 exhibit significant structural and functional differences. A $\beta$ 42 has a higher propensity to form fibrils, but it also produces oligomers with distinct structures from fibrils, leading to its toxic effects. Conversely, A $\beta$ 40 oligomers tend to adopt a linear configuration when exceeding tetramers, but their specific structure, particularly the dynamics of the C-terminal region, reducing their fibril-forming tendency. The structural disparities of beta amyloids influence their interactions with membranes, with the toxic effects on membranes primarily attributed to the oligomers of A $\beta$ 42. Aging and AD-related changes in membranes make them vulnerable to damage induced by amyloid. Additionally, disruption of copper homeostasis increases cholesterol and amyloid production, and stabilizes toxic oligomeric species that exacerbate membrane damage. The efficacy

of medications that stabilize small, harmless aggregates, preventing the formation of larger toxic species, supports the toxic oligomer hypothesis.

#### **Author contributions**

SB: Conceptualization, Investigation, Visualization, Writing – original draft, Writing – review and editing. LS: Conceptualization, Writing – review and editing.

# **Funding**

The author(s) declare that no financial support was received for the research and/or publication of this article.

#### Conflict of interest

The authors declare that the research was conducted in the absence of any commercial or financial relationships that could be construed as a potential conflict of interest.

The author(s) declared that they were an editorial board member of Frontiers, at the time of submission. This had no impact on the peer review process and the final decision.

#### Generative AI statement

The author(s) declare that no Generative AI was used in the creation of this manuscript.

Any alternative text (alt text) provided alongside figures in this article has been generated by Frontiers with the support of artificial intelligence and reasonable efforts have been made to ensure accuracy, including review by the authors wherever possible. If you identify any issues, please contact us.

#### Publisher's note

All claims expressed in this article are solely those of the authors and do not necessarily represent those of their affiliated organizations, or those of the publisher, the editors and the reviewers. Any product that may be evaluated in this article, or claim that may be made by its manufacturer, is not guaranteed or endorsed by the publisher.

#### References

Ahmed, M., Davis, J., Aucoin, D., Sato, T., Ahuja, S., Aimoto, S., et al. (2010). Structural conversion of neurotoxic amyloid-beta(1-42) oligomers to fibrils. *Nat. Struct. Mol. Biol.* 17, 561–567. doi:10.1038/nsmb.1799

Ahyayauch, H., Masserini, M. E., Goñi, F. M., and Alonso, A. (2024). The influence of lipid electric charge on the binding of A $\beta$ (1-42) amyloid peptide to bilayers in the liquid-ordered state. *Biomolecules* 14, 298. doi:10.3390/biom14030298

Arutyunyan, A., Seuma, M., Faure, A. J., Bolognesi, B., and Lehner, B. (2025). Massively parallel genetic perturbation suggests the energetic structure of an amyloid-β transition state. *Sci. Adv.* 11, eadv1422. doi:10.1126/sciadv.adv1422

Azouz, M., Cullin, C., Lecomte, S., and Lafleur, M. (2019). Membrane domain modulation of  $A\beta1-42$  oligomer interactions with supported lipid bilayers: an atomic force microscopy investigation. *Nanoscale* 11, 20857–20867. doi:10.1039/c9nr06361g

- Bagheri, S., and Saboury, A. A. (2022). "Chapter 18 kinase inhibition in Alzheimer's disease," in *Protein kinase inhibitors*. Editors M. I. Hassan, and S. Noor (Academic Press), 505–533.
- Bagheri, S., Squitti, R., Haertlé, T., Siotto, M., and Saboury, A. A. (2018). Role of copper in the onset of alzheimer's disease compared to other metals. *Front. Aging Neurosci.* 9, 446. doi:10.3389/fnagi.2017.00446
- Bagheri, S., Saboury, A. A., Haertlé, T., Rongioletti, M., and Saso, L. (2022). Probable reasons for neuron copper deficiency in the brain of patients with alzheimer's disease: the complex role of amyloid. *Inorganics* 10, 6. doi:10.3390/inorganics10010006
- Bagheri, S., Saboury, A. A., and Saso, L. (2024). Sequence of molecular events in the development of alzheimer's disease: cascade interactions from beta-amyloid to other involved proteins. Cells 13, 1293. doi:10.3390/cells13151293
- Banerjee, S., Hashemi, M., Lv, Z., Maity, S., Rochet, J.-C., and Lyubchenko, Y. L. (2017). A novel pathway for amyloids self-assembly in aggregates at nanomolar concentration mediated by the interaction with surfaces. *Sci. Rep.* 7, 45592. doi:10.1038/srep45592
- Barykin, E. P., Petrushanko, I. Y., Kozin, S. A., Telegin, G. B., Chernov, A. S., Lopina, O. D., et al. (2018). Phosphorylation of the amyloid-beta peptide inhibits zinc-dependent aggregation, prevents Na,K-ATPase inhibition, and reduces cerebral plaque deposition. *Front. Mol. Neurosci.* 11, 302. doi:10.3389/fnmol.2018.00302
- Barz, B., Buell, A. K., and Nath, S. (2021). Compact fibril-like structure of amyloid  $\beta$ -peptide (1-42) monomers. *Chem. Comm.* 57, 947–950. doi:10.1039/d0cc06607a
- Bera, S., Gayen, N., Mohid, S. A., Bhattacharyya, D., Krishnamoorthy, J., Sarkar, D., et al. (2020). Comparison of synthetic neuronal model membrane mimics in amyloid aggregation at atomic resolution. *ACS Chem. Neurosci.* 11, 1965–1977. doi:10.1021/acschemneuro.0c00166
- Bhowmik, D., Mote, K. R., MacLaughlin, C. M., Biswas, N., Chandra, B., Basu, J. K., et al. (2015). Cell-membrane-mimicking lipid-coated nanoparticles confer raman enhancement to membrane proteins and reveal membrane-attached Amyloid- $\beta$  conformation. ACS Nano 9, 9070–9077. doi:10.1021/acsnano.5b03175
- Bishop, G. M., and Robinson, S. R. (2004). Physiological roles of amyloid-beta and implications for its removal in alzheimer's disease. *Drugs Aging* 21, 621–630. doi:10.2165/00002512-200421100-00001
- Bitan, G., Kirkitadze, M. D., Lomakin, A., Vollers, S. S., Benedek, G. B., and Teplow, D. B. (2003). Amyloid beta -protein (abeta) assembly: Abeta 40 and abeta 42 oligomerize through distinct pathways. *Proc. Natl. Acad. Sci.* 100, 330–335. doi:10.1073/pnas.222681699
- Bode, D. C., Baker, M. D., and Viles, J. H. (2017). Ion channel formation by Amyloid- $\beta$ 42 oligomers but not Amyloid- $\beta$ 40 in cellular membranes. *J. Biol. Chem.* 292, 1404–1413. doi:10.1074/jbc.M116.762526
- Bokvist, M., Lindström, F., Watts, A., and Gröbner, G. (2004). Two types of alzheimer's β-Amyloid (1–40) peptide membrane interactions: aggregation preventing transmembrane anchoring *versus* accelerated surface fibril formation. *J. Mol. Biol.* 335, 1039–1049. doi:10.1016/j.jmb.2003.11.046
- Brender, J. R., Ghosh, A., Kotler, S. A., Krishnamoorthy, J., Bera, S., Morris, V., et al. (2019). Probing transient non-native states in amyloid beta fiber elongation by NMR. *Chem. Commun.* 55, 4483–4486. doi:10.1039/c9cc01067j
- Breydo, L., Kurouski, D., Rasool, S., Milton, S., Wu, J. W., Uversky, V. N., et al. (2016). Structural differences between amyloid beta oligomers. *Biochem. Biophys. Res. Commun.* 477, 700–705. doi:10.1016/j.bbrc.2016.06.122
- Burke, K. A., Yates, E. A., and Legleiter, J. (2013). Biophysical insights into how surfaces, including lipid membranes, modulate protein aggregation related to neurodegeneration. *Front. Neurol.* 4, 17. doi:10.3389/fneur.2013.00017
- Chandra, B., Maity, B. K., Das, A., and Maiti, S. (2018). Fluorescence quenching by lipid encased nanoparticles shows that amyloid- $\beta$  has a preferred orientation in the membrane. *Chem. Commun.* 54, 7750–7753. doi:10.1039/c8cc02108b
- Chen, G. F., Xu, T. H., Yan, Y., Zhou, Y. R., Jiang, Y., Melcher, K., et al. (2017). Amyloid beta: structure, biology and structure-based therapeutic development. *Acta Pharmacol. Sin.* 38, 1205–1235. doi:10.1038/aps.2017.28
- Connelly, L., Jang, H., Teran Arce, F., Capone, R., Kotler, S. A., Ramachandran, S., et al. (2012). Atomic force microscopy and MD simulations reveal pore-like structures of All-d-Enantiomer of alzheimer's  $\beta$ -Amyloid peptide: relevance to the ion channel mechanism of AD pathology. *J. Phys. Chem. B* 116, 1728–1735. doi:10.1021/jp2108126
- Dammers, C., Gremer, L., Reiß, K., Klein, A. N., Neudecker, P., Hartmann, R., et al. (2015). Structural analysis and aggregation propensity of pyroglutamate A $\beta$ (3-40) in aqueous trifluoroethanol. *PLoS One* 10, e0143647. doi:10.1371/journal.pone.0143647
- Dammers, C., Reiss, K., Gremer, L., Lecher, J., Ziehm, T., Stoldt, M., et al. (2017). Pyroglutamate-modified Amyloid- $\beta$ (3-42) shows  $\alpha$ -Helical intermediates before amyloid formation. *Biophys. J.* 112, 1621–1633. doi:10.1016/j.bpj.2017.03.007
- Demuro, A., Smith, M., and Parker, I. (2011). Single-channel Ca(2+) imaging implicates A $\beta$ 1-42 amyloid pores in alzheimer's disease pathology. *J. Cell Biol.* 195, 515–524. doi:10.1083/jcb.201104133
- Dey, A., Patil, A., Arumugam, S., and Maiti, S. (2024). Single-molecule maps of membrane insertion by Amyloid- $\beta$  oligomers predict their toxicity. *J. Phys. Chem. Lett.* 15, 6292–6298. doi:10.1021/acs.jpclett.4c01048

- Dias, C. L., Jalali, S., Yang, Y., and Cruz, L. (2020). Role of cholesterol on binding of amyloid fibrils to lipid bilayers. *J. Phys. Chem. B* 124, 3036–3042. doi:10.1021/acs.jpcb.0c00485
- Drolle, E., Negoda, A., Hammond, K., Pavlov, E., and Leonenko, Z. (2017). Changes in lipid membranes May trigger amyloid toxicity in alzheimer's disease. *PLoS One* 12, e0182194. doi:10.1371/journal.pone.0182194
- Ewald, M., Henry, S., Lambert, E., Feuillie, C., Bobo, C., Cullin, C., et al. (2019). High speed atomic force microscopy to investigate the interactions between toxic  $A\beta1-42$  peptides and model membranes in real time: impact of the membrane composition. *Nanoscale* 11, 7229–7238. doi:10.1039/c8nr08714h
- Fabelo, N., Martín, V., Marín, R., Moreno, D., Ferrer, I., and Díaz, M. (2014). Altered lipid composition in cortical lipid rafts occurs at early stages of sporadic alzheimer's disease and facilitates APP/BACE1 interactions. *Neurobiol. Aging* 35, 1801–1812. doi:10.1016/j.neurobiolaging.2014.02.005
- Feuillie, C., Lambert, E., Ewald, M., Azouz, M., Henry, S., Marsaudon, S., et al. (2020). High speed AFM and NanoInfrared spectroscopy investigation of A $\beta$ (1-42) peptide variants and their interaction with POPC/SM/Chol/GM1 model membranes. *Front. Mol. Biosci.* 7, 571696. doi:10.3389/fmolb.2020.571696
- Gardon, L., Becker, N., Gremer, L., and Heise, H. (2024). Structural impact of N-terminal pyroglutamate in an Amyloid- $\beta$ (3-42) fibril probed by solid-state NMR spectroscopy. *Chemistry* 30, e202303007. doi:10.1002/chem.202303007
- Ghosh, U., Thurber, K. R., Yau, W. M., and Tycko, R. (2021). Molecular structure of a prevalent amyloid- $\beta$  fibril polymorph from alzheimer's disease brain tissue. *Proc. Natl. Acad. Sci.* 118, e2023089118. doi:10.1073/pnas.2023089118
- Glabe, C. G. (2008). Structural classification of toxic amyloid oligomers. *J. Biol. Chem.* 283, 29639–29643. doi:10.1074/jbc.R800016200
- Gu, L., and Guo, Z. (2013). Alzheimer's A $\beta$ 42 and A $\beta$ 40 peptides form interlaced amyloid fibrils. *J. Neurochem.* 126, 305–311. doi:10.1111/jnc.12202
- Heermant, S., Paschke, R., and Kozuch, J. (2025). Antiparallel to parallel  $\beta$ -Sheet transition of Amyloid- $\beta$  is promoted by the ability to incorporate into membranes. Available online at: https://chemrxiv.org/engage/chemrxiv/article-details/67b2445981d2151a02c02478.
- Hellström-Lindahl, E., Viitanen, M., and Marutle, A. (2009). Comparison of abeta levels in the brain of familial and sporadic alzheimer's disease. *Neurochem. Int.* 55, 243–252. doi:10.1016/j.neuint.2009.03.007
- Heo, C. E., Park, C. R., and Kim, H. I. (2021). Effect of packing density of lipid vesicles on the A $\beta$ 42 fibril polymorphism. *Chem. Phys. Lipids* 236, 105073. doi:10.1016/j.chemphyslip.2021.105073
- Hu, Z.-W., Vugmeyster, L., Au, D. F., Ostrovsky, D., Sun, Y., and Qiang, W. (2019). Molecular structure of an N-terminal phosphorylated  $\beta$ -amyloid fibril. *Proc. Natl. Acad. Sci.* 116, 11253–11258. doi:10.1073/pnas.1818530116
- Hu, Z. W., Au, D. F., Cruceta, L., Vugmeyster, L., and Qiang, W. (2020). N-Terminal modified  $A\beta$  variants enable modulations to the structures and cytotoxicity levels of wild-type  $A\beta$  fibrils through cross-seeding. *ACS Chem. Neurosci.* 11, 2058–2065. doi:10.1021/acschemneuro.0c00316
- Huang, Y. R., and Liu, R. T. (2020). The toxicity and polymorphism of  $\beta$ -Amyloid oligomers. *Int. J. Mol. Sci.* 21, 4477. doi:10.3390/ijms21124477
- Iwatsubo, T., Odaka, A., Suzuki, N., Mizusawa, H., Nukina, N., and Ihara, Y. (1994). Visualization of A $\beta$ 42(43) and A $\beta$ 40 in senile plaques with end-specific A $\beta$  monoclonals: evidence that an initially deposited species is A $\beta$ 42(43). Neuron 13, 45–53. doi:10.1016/0896-6273(94)90458-8
- Jamasbi, E., Separovic, F., Hossain, M. A., and Ciccotosto, G. D. (2017). Phosphorylation of a full length amyloid- $\beta$  peptide modulates its amyloid aggregation, cell binding and neurotoxic properties. *Mol. Biosyst.* 13, 1545–1551. doi:10.1039/c7mb00249a
- Jan, A., Gokce, O., Luthi-Carter, R., and Lashuel, H. A. (2008). The ratio of monomeric to aggregated forms of Abeta40 and Abeta42 is an important determinant of amyloid-beta aggregation, fibrillogenesis, and toxicity. *J. Biol. Chem.* 283, 28176–28189. doi:10.1074/jbc.M803159200
- Jin, L., Wu, W.-H., Li, Q.-Y., Zhao, Y.-F., and Li, Y.-M. (2011). Copper inducing A $\beta$ 42 rather than A $\beta$ 40 nanoscale oligomer formation is the key process for A $\beta$  neurotoxicity. *Nanoscale* 3, 4746–4751. doi:10.1039/c1nr11029b
- John, T., Piantavigna, S., Dealey, T. J. A., Abel, B., Risselada, H. J., and Martin, L. L. (2023). Lipid oxidation controls peptide self-assembly near membranes through a surface attraction mechanism. *Chem. Sci.* 14, 3730–3741. doi:10.1039/d3sc00159h
- Johnson, R. D., Schauerte, J. A., Chang, C. C., Wisser, K. C., Althaus, J. C., Carruthers, C. J., et al. (2013). Single-molecule imaging reveals aβ42:aβ40 ratio-dependent oligomer growth on neuronal processes. *Biophys. J.* 104, 894–903. doi:10.1016/j.bpj.2012. 12.051
- Kayed, R., Pensalfini, A., Margol, L., Sokolov, Y., Sarsoza, F., Head, E., et al. (2009). Annular protofibrils are a structurally and functionally distinct type of amyloid oligomer. *J. Biol. Chem.* 284, 4230–4237. doi:10.1074/jbc.M808591200
- Kelleher, R. J., 3rd, and Shen, J. (2017). Presenilin-1 mutations and alzheimer's disease. Proc. Natl. Acad. Sci. 114, 629–631. doi:10.1073/pnas.1619574114

- Khaled, M., Rönnbäck, I., Ilag, L. L., Gräslund, A., Strodel, B., and Österlund, N. (2023). A hairpin motif in the Amyloid- $\beta$  peptide is important for formation of disease-related oligomers. *J. Am. Chem. Soc.* 145, 18340–18354. doi:10.1021/jacs.3c03980
- Kohoutek, K. M., and Harrington, P. B. (2023). Electrospray ionization ion mobility mass spectrometry. *Crit. Rev. Anal. Chem.* 53, 483–497. doi:10.1080/10408347.2021.1964938
- Kotler, S. A. (2015). Biophysical insights into the role of amyloid-beta misfolding in alzheimer's disease pathogenesis, biophysics. Ann Arbor, Michigan: University of Michigan, 143.
- Kumar, S., Rezaei-Ghaleh, N., Terwel, D., Thal, D. R., Richard, M., Hoch, M., et al. (2011). Extracellular phosphorylation of the amyloid  $\beta$ -peptide promotes formation of toxic aggregates during the pathogenesis of alzheimer's disease. *Embo J.* 30, 2255–2265. doi:10.1038/emboj.2011.138
- Kumar, S., Lemere, C. A., and Walter, J. (2020). Phosphorylated A $\beta$  peptides in human Down syndrome brain and different alzheimer's-like mouse models. *Acta Neuropathol. Commun.* 8, 118. doi:10.1186/s40478-020-00959-w
- Kunnath Muhammedkutty, F. N., and Zhou, H.-X. (2025). Membrane-assisted Aβ40 aggregation pathways. *Cell Rep. Phys. Sci.* 6, 102436. doi:10.1016/j.xcrp.2025.102436
- Kuperstein, I., Broersen, K., Benilova, I., Rozenski, J., Jonckheere, W., Debulpaep, M., et al. (2010). Neurotoxicity of alzheimer's disease A $\beta$  peptides is induced by small changes in the A $\beta$ 42 to A $\beta$ 40 ratio. *Embo J.* 29, 3408–3420. doi:10.1038/emboj.2010.211
- Lal, R., Lin, H., and Quist, A. P. (2007). Amyloid beta ion channel: 3D structure and relevance to amyloid channel paradigm. *Biochim. Biophys. Acta* 1768, 1966–1975. doi:10.1016/j.bbamem.2007.04.021
- Lee, M., Yau, W.-M., Louis, J. M., and Tycko, R. (2023). Structures of brain-derived 42-residue amyloid- $\beta$  fibril polymorphs with unusual molecular conformations and intermolecular interactions. *Proc. Natl. Acad. Sci.* 120, e2218831120. doi:10.1073/pnas.2218831120
- Leite, J. P., Gimeno, A., Taboada, P., Jiménez-Barbero, J. J., and Gales, L. (2020). Dissection of the key steps of amyloid- $\beta$  peptide 1-40 fibrillogenesis. *Int. J. Biol. Macromol.* 164, 2240–2246. doi:10.1016/j.ijbiomac.2020.08.023
- Liu, P. P., Xie, Y., Meng, X.-Y., and Kang, J.-S. (2019). History and progress of hypotheses and clinical trials for Alzheimer's disease. *Signal Transduct. Target Ther.* 4, 29. doi:10.1038/s41392-019-0063-8
- Lührs, T., Ritter, C., Adrian, M., Riek-Loher, D., Bohrmann, B., Döbeli, H., et al. (2005). 3D structure of Alzheimer's amyloid-beta(1-42) fibrils. *Proc. Natl. Acad. Sci.* 102, 17342–17347. doi:10.1073/pnas.0506723102
- Lv, Z., Roychaudhuri, R., Condron, M. M., Teplow, D. B., and Lyubchenko, Y. L. (2013). Mechanism of amyloid  $\beta$ -protein dimerization determined using single-molecule AFM force spectroscopy. *Sci. Rep.* 3, 2880. doi:10.1038/srep02880
- Lyubchenko, Y. L. (2020). Amyloid B-Protein aggregation at physiologically relevant concentrations. A critical role of membranes. *Alzheimers Res. Ther. Open Access* 3, 114.
- Lyubchenko, Y. (2023). Amyloid cascade hypothesis for Alzheimer's disease. Does it work under physiological conditions? *Precis. Nanomed* 6. doi:10.33218/001c.77826
- Mamone, S., Glöggler, S., Becker, S., and Rezaei-Ghaleh, N. (2021). Early divergence in misfolding pathways of amyloid-beta peptides. *Chem. Phys. Chem.* 22, 2158–2163. doi:10.1002/cphc.202100542
- Meker, S., Chin, H., Sut, T. N., and Cho, N. J. (2018). Amyloid- $\beta$  peptide triggers membrane remodeling in supported lipid bilayers depending on their hydrophobic thickness. *Langmuir* 34, 9548–9560. doi:10.1021/acs.langmuir.8b01196
- Meng, F., Kim, J.-Y., Louis, J. M., and Chung, H. S. (2024). Single-molecule characterization of heterogeneous oligomer formation during Co-Aggregation of 40- and 42-Residue Amyloid- $\beta$ . J. Am. Chem. Soc. 146, 24426–24439. doi:10.1021/iacs.4c06372
- Miller, D. L., Papayannopoulos, I. A., Styles, J., Bobin, S. A., Lin, Y. Y., Biemann, K., et al. (1993). Peptide compositions of the cerebrovascular and senile plaque core amyloid deposits of alzheimer's disease. *Arch. Biochem. Biophys.* 301, 41–52. doi:10.1006/abbi.1993.1112
- Moro, M. L., Phillips, A. S., Gaimster, K., Paul, C., Mudher, A., Nicoll, J. A. R., et al. (2018). Pyroglutamate and isoaspartate modified amyloid-beta in ageing and alzheimer's disease. *Acta Neuropathol. Commun.* 6, 3. doi:10.1186/s40478-017-0505-x
- Mukherjee, S., Perez, K. A., Lago, L. C., Klatt, S., McLean, C. A., Birchall, I. E., et al. (2021). Quantification of N-terminal amyloid-β isoforms reveals isomers are the Most abundant form of the amyloid-β peptide in sporadic alzheimer's disease. *Brain Commun.* 3, fcab028. doi:10.1093/braincomms/fcab028
- Nag, S., Sarkar, B., Chandrakesan, M., Abhyanakar, R., Bhowmik, D., Kombrabail, M., et al. (2013). A folding transition underlies the emergence of membrane affinity in amyloid- $\beta$ . *Phys. Chem. Chem. Phys.* 15, 19129–19133. doi:10.1039/c3cp52732h
- Nakano, H., Hikishima, S., Mori, M., Minamikawa, J., Muramatsu, D., Sakashita, Y., et al. (2025). Globular-shaped  $A\beta$  oligomers have diverse mechanisms for promoting  $A\beta$  aggregations with the facilitation of fibril elongation. *Neurobiol. Dis.* 205, 106775. doi:10.1016/j.nbd.2024.106775
- Nath, S., Buell, A. K., and Barz, B. (2023). Pyroglutamate-modified amyloid  $\beta(3-42)$  monomer has more  $\beta$ -sheet content than the amyloid  $\beta(1-42)$  monomer. *Phys. Chem. Chem. Phys.* 25, 16483–16491. doi:10.1039/d2cp05961d

- Nguyen, H. L., Linh, H. Q., Krupa, P., La Penna, G., and Li, M. S. (2022). Amyloid  $\beta$  dodecamer disrupts the neuronal membrane more strongly than the mature fibril: understanding the role of oligomers in neurotoxicity. *J. Phys. Chem. B* 126, 3659–3672. doi:10.1021/acs.jpcb.2c01769
- Niu, Z., Zhang, Z., Zhao, W., and Yang, J. (2018). Interactions between amyloid  $\beta$  peptide and lipid membranes. *Biochim. Biophys. Acta Biomembr.* 1860, 1663–1669. doi:10.1016/j.bbamem.2018.04.004
- Owen, M. C., Kulig, W., Poojari, C., Rog, T., and Strodel, B. (2018). Physiologically-relevant levels of sphingomyelin, but not GM1, induces a  $\beta$ -sheet-rich structure in the amyloid- $\beta$ (1-42) monomer. *Biochim. Biophys. Acta Biomembr.* 1860, 1709–1720. doi:10.1016/j.bbamem.2018.03.026
- Pauwels, K., Williams, T. L., Morris, K. L., Jonckheere, W., Vandersteen, A., Kelly, G., et al. (2012). Structural basis for increased toxicity of pathological aβ42:aβ40 ratios in alzheimer disease. *J. Biol. Chem.* 287, 5650–5660. doi:10.1074/jbc.M111.264473
- Press-Sandler, O., and Miller, Y. (2022). Molecular insights into the primary nucleation of polymorphic amyloid  $\beta$  dimers in DOPC lipid bilayer membrane. *Protein Sci.* 31, e4283. doi:10.1002/pro.4283
- Pujol-Pina, R., Vilaprinyó-Pascual, S., Mazzucato, R., Arcella, A., Vilaseca, M., Orozco, M., et al. (2015). SDS-PAGE analysis of A $\beta$  oligomers is disserving research into Alzheimer's disease: appealing for ESI-IM-MS. *Sci. Rep.* 5, 14809. doi:10.1038/srep14809
- Quist, A., Doudevski, I., Lin, H., Azimova, R., Ng, D., Frangione, B., et al. (2005). Amyloid ion channels: a common structural link for protein-misfolding disease. *Proc. Natl. Acad. Sci.* 102, 10427–10432. doi:10.1073/pnas.0502066102
- Rijal Upadhaya, A., Kosterin, I., Kumar, S., von Arnim, C. A., Yamaguchi, H., Fändrich, M., et al. (2014). Biochemical stages of amyloid- $\beta$  peptide aggregation and accumulation in the human brain and their association with symptomatic and pathologically preclinical alzheimer's disease. Brain 137, 887–903. doi:10.1093/brain/awt362
- Robinson, J., Sarangi, N. K., and Keyes, T. E. (2023). Role of phosphatidylserine in amyloid-beta oligomerization at asymmetric phospholipid bilayers. *Phys. Chem. Chem. Phys.* 25, 7648–7661. doi:10.1039/d2cp03344e
- Robinson, M., Payton, O., Picco, L., Beazely, M., Miles, M., and Leonenko, Z. (2025). Contact mode high-speed AFM of phase separated lipid bilayers to study Amyloid-β interactions. Available online at: https://www.biorxiv.org/content/10.1101/2025.01.14.633021v1
- Roher, A. E., Lowenson, J. D., Clarke, S., Wolkow, C., Wang, R., Cotter, R. J., et al. (1993). Structural alterations in the peptide backbone of beta-amyloid core protein May account for its deposition and stability in alzheimer's disease. *J. Biol. Chem.* 268, 3072–3083. doi:10.1016/s0021-9258(18)53661-9
- Roher, A. E., Kokjohn, T. A., Clarke, S. G., Sierks, M. R., Maarouf, C. L., Serrano, G. E., et al. (2017). APP/A $\beta$  structural diversity and alzheimer's disease pathogenesis. *Neurochem. Int.* 110, 1–13. doi:10.1016/j.neuint.2017.08.007
- Ryan, T. M., Roberts, B. R., McColl, G., Hare, D. J., Doble, P. A., Li, Q. X., et al. (2015). Stabilization of nontoxic A $\beta$ -oligomers: insights into the mechanism of action of hydroxyquinolines in alzheimer's disease. *J. Neurosci.* 35, 2871–2884. doi:10.1523/JNEUROSCI.2912-14.2015
- Sarkar, B., Das, A. K., and Maiti, S. (2013). Thermodynamically stable amyloid- $\beta$  monomers have much lower membrane affinity than the small oligomers. *Front. Physiol.* 4, 84. doi:10.3389/fphys.2013.00084
- Schäffler, M., Wales, D. J., and Strodel, B. (2024). The energy landscape of A $\beta$ 42: a funnel to disorder for the monomer becomes a folding funnel for self-assembly. *Chem. Commun.* 60, 13574–13577. doi:10.1039/d4cc02856b
- Schauerte, J. A., Wong, P. T., Wisser, K. C., Ding, H., Steel, D. G., and Gafni, A. (2010). Simultaneous single-molecule fluorescence and conductivity studies reveal distinct classes of abeta species on lipid bilayers. *Biochemistry* 49, 3031–3039. doi:10.1021/bi901444w
- Scheidt, H., Adler, J., Krueger, M., and Huster, D. (2016). Fibrils of truncated pyroglutamyl-modified A? Peptide exhibit a similar structure as wildtype mature A? Fibrils. Sci. Rep. 6, 33531. doi:10.1038/srep33531
- Scheidt, H. A., Adler, J., Zeitschel, U., Höfling, C., Korn, A., Krueger, M., et al. (2017). Pyroglutamate-modified amyloid  $\beta$  (11- 40) fibrils are more toxic than wildtype fibrils but structurally very similar. *Chemistry* 23, 15834–15838. doi:10.1002/chem.201703909
- Scheidt, H., Das, A., Korn, A., Krüger, M., Maiti, S., and Huster, D. (2020). Structural characteristics of oligomers formed by pyroglutamate-modified amyloid  $\beta$  peptides studied by solid-state NMR. *Phys. Chem. Chem. Phys.* 22, 16887–16895. doi:10.1039/d0cp02307h
- Scheidt, H. A., Korn, A., Schwarze, B., Krueger, M., and Huster, D. (2024). Conformation of pyroglutamated amyloid  $\beta$  (3–40) and (11–40) fibrils extended or hairpin? *J. Phys. Chem. B* 128, 1647–1655. doi:10.1021/acs.jpcb.3c07285
- Schmidt, M., Sachse, C., Richter, W., Xu, C., Fändrich, M., and Grigorieff, N. (2009). Comparison of alzheimer Abeta(1-40) and Abeta(1-42) amyloid fibrils reveals similar protofilament structures. *Proc. Natl. Acad. Sci.* 106, 19813–19818. doi:10.1073/pnas.0905007106
- Schrempel, S., Kottwitz, A. K., Piechotta, A., Gnoth, K., Büschgens, L., Hartlage-Rübsamen, M., et al. (2024). Identification of isoAsp7-A $\beta$  as a major A $\beta$  variant

in alzheimer's disease, dementia with lewy bodies and vascular dementia. Acta Neuropathol. 148, 78. doi:10.1007/s00401-024-02824-9

Sgourakis, N. G., Yan, Y., McCallum, S. A., Wang, C., and Garcia, A. E. (2007). The Alzheimer's peptides Abeta40 and 42 adopt distinct conformations in water: a combined MD/NMR study. *J. Mol. Biol.* 368, 1448–1457. doi:10.1016/j.jmb.2007.02.093

Sunil Menon, R., Wolynes, P. G., and Vekilov, P. G. (2025). Direct observation of Amyloid- $\beta$  42 oligomer, fibril, and amorphous aggregate growth and dissolution at biomimetic concentrations. *J. Phys. Chem. B* 129, 9083–9096. doi:10.1021/acs.jpcb.5c03842

Tay, W. M., Huang, D., Rosenberry, T. L., and Paravastu, A. K. (2013). The Alzheimer's amyloid- $\beta$ (1-42) peptide forms off-pathway oligomers and fibrils that are distinguished structurally by intermolecular organization. *J. Mol. Biol.* 425, 2494–2508. doi:10.1016/j.jmb.2013.04.003

Tehrani, M. J., Matsuda, I., Yamagata, A., Kodama, Y., Matsunaga, T., Sato, M., et al. (2024). E22G A $\beta$ 40 fibril structure and kinetics illuminate how A $\beta$ 40 rather than A $\beta$ 42 triggers familial Alzheimer's. *Nat. Commun.* 15, 7045. doi:10.1038/s41467-024-51294-w

Terrill-Usery, S. E., Colvin, B. A., Davenport, R. E., and Nichols, M. R. (2016). A $\beta$ 40 has a subtle effect on A $\beta$ 42 protofibril formation, but to a lesser degree than A $\beta$ 42 concentration, in A $\beta$ 42/A $\beta$ 40 mixtures. *Arch. Biochem. Biophys.* 597, 1–11. doi:10.1016/j.abb.2016.03.017

Tian, Y., Shang, Q., Liang, R., and Viles, J. H. (2024). Copper(II) can kinetically trap arctic and Italian Amyloid- $\beta$ (40) as toxic oligomers, mimicking Cu(II) binding to wild-type Amyloid- $\beta$ (42): implications for familial alzheimer's disease. *J. Am. Chem. Soc.* 4, 578–591. doi:10.1021/jacsau.3c00687

Vadukul, D. M., Maina, M., Franklin, H., Nardecchia, A., Serpell, L. C., and Marshall, K. E. (2020). Internalisation and toxicity of amyloid- $\beta$  1-42 are influenced by its conformation and assembly state rather than size. *FEBS Lett.* 594, 3490–3503. doi:10.1002/1873-3468.13919

van Deventer, R., and Lyubchenko, Y. L. (2024). Damage of the phospholipid bilayer by A $\beta$ 42 at physiologically relevant peptide concentrations. ACS Chem. Neurosci. 15, 4559–4567. doi:10.1021/acschemneuro.4c00647

Varshavskaya, K. B., Petrushanko, I. Y., Mitkevich, V. A., Barykin, E. P., and Makarov, A. A. (2024). Post-translational modifications of beta-amyloid alter its transport in the blood-brain barrier *in vitro* model. *Front. Mol. Neurosci.* 17, 1362581. doi:10.3389/fnmol.2024.1362581

Wälti, M. A., Ravotti, F., Arai, H., Glabe, C. G., Wall, J. S., Böckmann, A., et al. (2016). Atomic-resolution structure of a disease-relevant  $A\beta(1-42)$  amyloid fibril. *Proc. Natl. Acad. Sci. U. S. A.* 113, E4976–E4984. doi:10.1073/pnas.1600749113

Watanabe-Nakayama, T., Ono, K., Itami, M., Takahashi, R., Teplow, D. B., and Yamada, M. (2016). High-speed atomic force microscopy reveals structural dynamics of amyloid β1-42 aggregates. *Proc. Natl. Acad. Sci.* 113, 5835–5840. doi:10.1073/pnas.1524807113

Xiao, Y., Ma, B., McElheny, D., Parthasarathy, S., Long, F., Hoshi, M., et al. (2015).  $A\beta(1-42)$  fibril structure illuminates self-recognition and replication of amyloid in alzheimer's disease. *Nat. Struct. Mol. Biol.* 22, 499–505. doi:10.1038/nsmb.2991

Yagi-Utsumi, M., Kanaoka, Y., Miyajima, S., Itoh, S. G., Yanagisawa, K., Okumura, H., et al. (2024). Single-molecule kinetic observation of antibody interactions with growing amyloid  $\beta$  fibrils. *J. Am. Chem. Soc.* 146, 31518–31528. doi:10.1021/jacs.

Yang, T., Li, S., Xu, H., Walsh, D. M., and Selkoe, D. J. (2017). Large soluble oligomers of amyloid  $\beta$ -Protein from alzheimer brain are far less neuroactive than the smaller oligomers to which they dissociate. *J. Neurosci.* 37, 152–163. doi:10.1523/JNEUROSCI.1698-16.2016

Yang, Y., Zhang, W., Murzin, A. G., Schweighauser, M., Huang, M., Lövestam, S., et al. (2023). Cryo-EM structures of amyloid- $\beta$  filaments with the arctic mutation (E22G) from human and mouse brains. *Acta Neuropathol.* 145, 325–333. doi:10.1007/s00401-022-02533-1

Yasumoto, T., Takamura, Y., Tsuji, M., Watanabe-Nakayama, T., Imamura, K., Inoue, H., et al. (2019). High molecular weight amyloid  $\beta(1-42)$  oligomers induce neurotoxicity via plasma membrane damage. Faseb J. 33, 9220–9234. doi:10.1096/fj. 201900604R

Zarrilli, B., Bonanni, R., Belfiore, M., Severino, M., Cariati, I., Fioravanti, R., et al. (2024). Molecular mechanisms at the basis of the protective effect exerted by EPPS on neurodegeneration induced by prefibrillar amyloid oligomers. *Sci. Rep.* 14, 26533. doi:10.1038/s41598-024-77859-9

Zhang, H., Ma, Q., Zhang, Y. W., and Xu, H. (2012). Proteolytic processing of Alzheimer's  $\beta$ -amyloid precursor protein. *J. Neurochem.* 120 (Suppl. 1), 9–21. doi:10.1111/j.1471-4159.2011.07519.x

Zhuang, W., Sgourakis, N. G., Li, Z., Garcia, A. E., and Mukamel, S. (2010). Discriminating early stage A{beta}42 monomer structures using chirality-induced 2DIR spectroscopy in a simulation study. *Proc. Natl. Acad. Sci.* 107, 15687–15692. doi:10.1073/pnas.1002131107

Zubillaga, M., Rosa, D., Astiz, M., Tricerri, M. A., and Arnal, N. (2022). Effect of Sublethal Copper Overload on Cholesterol *de novo* Synthesis in Undifferentiated Neuronal Cells. *ACS Omega* 7, 25022–25030. doi:10.1021/acsomega. 2c00703